# Behaviour and residual compression resistances of circular high strength concrete-filled stainless steel tube (HCFSST) stub columns after exposure to fire

An He [a], Yating Liang [b], Ou Zhao [*a]

[a] School of Civil and Environmental Engineering, Nanyang Technological University, Singapore

[b] School of Engineering, University of Glasgow, Glasgow, UK

[*] Corresponding author, Email: ou.zhao@ntu.edu.sg

**Abstract:** The structural behaviour and residual compression resistances of circular high strength concrete-filled stainless steel tube (HCFSST) stub columns after exposure to fire were experimentally and numerically investigated in this paper. The experimental study was performed on 12 circular HCFSST stub column specimens after exposure to the ISO-834 standard fire for three levels of heating durations (15 min, 30 min and 45 min) as well as 4 unheated circular HCFSST stub column specimens (i.e. reference specimens). The experimental study was supplemented by a numerical modelling study, where two types of finite element (FE) models, namely heat transfer and mechanical FE models, were firstly developed to simulate the thermal and mechanical responses of the circular HCFSST stub column specimens, and then used to perform parametric studies to derive additional numerical results. Due to the lack of existing design codes for concrete-filled stainless steel tube members and concrete-filled carbon steel tube members after exposure to fire, the corresponding codified design provisions for circular concrete-filled carbon steel tube members at room temperature, as established in Europe, Australia and America, were evaluated for their suitability to circular HCFSST stub columns after exposure to fire, based on the test and numerical parametric study

results. It was generally found that both the European and Australian codes yield a high level of accuracy and consistency in predicting the residual compression resistances of circular HCFSST stub columns after exposure to fire, while the American specification leads to rather conservative and scattered design residual compression resistances.

## 1. Introduction

The past decade has witnessed an increasing trend of utilising concrete-filled stainless steel tube (CFSST) composite columns in civil and offshore engineering applications. Compared with the conventional concrete-filled carbon steel tube columns, the novel CFSST columns possess more favourable mechanical characteristics, including larger load-carrying capacity and higher ductility, owing principally to the superior material properties (high strength and excellent ductility) of stainless steel [1]. Moreover, the resistance against corrosion of stainless steel is significantly better than that of carbon steel, and thus CFSST columns require little or no maintenance work during their service life cycle, in comparison with concrete-filled carbon steel tube columns, where regular maintenance such as the spray of anti-corrosive coatings on the outer carbon steel tubes is generally required over the whole service life. Experimental investigations have been previously performed on various types of circular CFSST column members, with a brief summary given below. Uy et al. [2] and Lam and Gardner [3] conducted tests on circular CFSST stub columns to examine their structural behaviour and cross-section compression resistances, while the behaviour and compression resistances of circular CFSST stub columns with novel types of concrete infill, such as recycled aggregate concrete and seawater and sea sand concrete, were studied by Yang and Ma [4], Li et al. [5] and Liao et al. [6]. The flexural buckling behaviour and resistances of circular CFSST long columns subjected to axial compression load were investigated by Uy et al. [2], based on a thorough experimental programme. Yang et al. [7] and Liao et al. [8] examined the hysteretic responses of circular CFSST long columns under lateral cyclic loading combined with constant axial compression force. Han et al. [9] and Tao et al. [10] respectively conducted experiments on circular CFSST long columns at elevated temperatures and after exposure to elevated temperatures, to investigate and quantify their residual flexural buckling strengths, and highlighted that the application of higher initial loads and arrangement of internal reinforcements are advantageous to the increase of the post-fire residual flexural buckling strengths of CFSST long columns. The brief review generally revealed that although extensive experimental studies have been carried out to investigate the static, hysteretic, fire and post-fire behaviour of circular CFSST column members, research into circular high strength concrete-filled stainless steel tube (HCFSST) columns at elevated temperatures and after exposure to elevated temperature remained scarce.

This paper reports a comprehensive experimental and finite element modelling programme to study the cross-section behaviour and residual compression capacities of circular HCFSST stub columns after exposure to fire. The experimental programme was performed on 12 circular HCFSST stub column specimens after exposure to the ISO-834 standard fire for three heating durations of 15 min, 30 min and 45 min as well as 4 unheated reference specimens, whilst the finite element modelling programme involved a simulation study to simulate the thermal and mechanical responses of the circular HCFSST stub column specimens and a parametric study to derive additional structural performance data over a broader range of cross-section dimensions. Due to the absence of established design standards for concrete-filled stainless steel tube members and concrete-filled carbon steel tube members after exposure to fire, the corresponding international design codes for concrete-filled carbon steel tube members at room temperature, including the European code EN 1994-1-1 [11], Australian Standard AS 5100 [12] and American Specifications AISC 360 [13], were evaluated for their suitability to the design of circular HCFSST stub columns after exposure to fire, based on the experimental and numerical data.

## 2. Experimental investigation

### *2.1 General*

A comprehensive experimental study was firstly performed to investigate the structural performance and residual compression resistances of circular HCFSST stub columns after exposure to fire. Sixteen HCFSST stub column specimens were employed in the testing programme, and designed such that the effect of a series of parameters, including the size of the outer stainless steel circular hollow tube, the concrete infill grade and the duration of heating, on the post-fire responses and resistances of circular HCFSST stub columns can be investigated. Two sizes of circular hollow section (CHS) tubes – CHS 73×3 and CHS 89×3 – fabricated from grade EN 1.4301 austenitic stainless steel, and two grades of high strength concrete infill – C90 and C140 – were adopted for fabricating four series of HCFSST stub column specimens, namely D73-C90, D73-C140, D89-C90 and D89-C140; the identifier of each specimen series begins with the nominal outer diameter of the austenitic stainless steel circular hollow tube, and ends with the grade of the high strength concrete infill. Each series contains four nominally identical HCFSST stub column specimens, with one unheated and another three exposed to the ISO-834 standard fire for heating durations of 15 min, 30 min and 45 min, and the identifier of each specimen comprises the specimen series and the heating duration, e.g., D73-C90-T30 represents a HCFSST stub column specimen with the outer tube of CHS 73×3 and high strength concrete infill of grade C90 after exposure to the ISO-834 standard fire for 30 min. The nominal length of each stub column specimen was chosen to be three times the nominal outer diameter of the austenitic stainless steel CHS tube, in order to preclude the occurrence of member global instability [14–18]. The measured geometric properties and heating duration of each HCFSST stub column specimen, including the outer diameter of the austenitic stainless steel CHS tube $D$, the wall thickness of the tube $t$, the stub column specimen length $L$ and the heating duration $T_h$, are presented in Table 1.

### *2.2 Heating and cooling process*

The circular HCFSST stub columns specimens, together with the coupons cut from the austenitic stainless steel CHS tubes, were heated in an electric furnace, where two rows of heating elements are distributed evenly over both sides of the chamber, as displayed in Fig. 1. The air temperature in the chamber was set to be increased following the ISO-834 standard fire curve [19], and three levels of heating durations (15 min, 30 min and 45 min) were considered for each specimen series. A series of temperature probes, located just behind the heating elements, were employed for the purpose of monitoring and controlling the furnace temperatures at various locations to follow the ISO-834 standard fire curve during heating [19]. High strength concrete is prone to explosive spalling [20], which may damage the heating elements of the furnace; therefore, the two ends of each circular HCFSST stub column specimen were welded with steel plates, in order to prevent the inner concrete from flying out during heating. It is worth noting that all the circular HCFSST stub column specimens were heated in an unloaded condition in the furnace, and the resulting post-fire residual strengths are generally lower (i.e. more conservative) than those derived from the specimens heated in a preload condition [21, 22]. During the heating process, four thermal couples were adopted to monitor the temperatures of both the austenitic stainless steel tube and high strength concrete infill of each HCFSST stub column specimen. Specifically, three thermocouples, inserted into the high strength concrete infill at the mid-height during the fabrication of the HCFSST stub column specimen, were arranged along the radial direction (see Fig. 2) to capture the uneven temperature field of the inner high strength concrete core, while an additional thermal couple was positioned at the outer face of the austenitic stainless steel tube to measure its surface temperature. Upon attainment of the pre-specified heating durations, the electric furnace was switched off, allowing the HCFSST stub column specimens and the coupons to be naturally cooled down to the room temperature. Welded end plates were then cut from the specimen ends.

The full temperature–time curves measured from the four thermal couples for the HCFSST stub column specimens of each test series are shown in Figs 3–6, respectively, together with the ISO-834 standard fire (temperature–time) curve. It is evident in Figs 3–6 that the temperatures of the outer austenitic stainless steel tubes of the HCFSST stub column specimens follow closely with the ISO-834 temperature–time curve during the heating process; the temperatures at the three measured positions of the high strength concrete infill are shown to have large difference and decrease as the measured location moves from 'Position 1' (just beside the inner face of the austenitic stainless steel tube) to 'Position 3' (centroid of the high strength concrete infill), which can be attributed to the high thermal capacity (and thus low heat transfer coefficient) of concrete. Table 1 reports the maximum attained temperatures at the three measured positions of the high strength concrete infill $T_1$, $T_2$ and $T_3$ and at the outer face of the austenitic stainless steel tube $T_4$ for each HCFSST stub column specimen.

The austenitic stainless steel displayed obvious changes in surface colour after exposure to fire. As exhibited in Fig. 7, the surface colour of austenitic stainless steel after exposure to the ISO-

834 standard fire for a duration of 15 min (leading to the surface temperature of 687 ℃) turned into dark red, while the colours of the surface respectively became dark grey and black after exposure to longer heating durations of 30 min and 45 min (leading to the surface temperatures of 817 ℃ and 881 ℃). In terms of the inner high strength concrete cores, their end surface colours all became whitish grey upon heating [23], as exhibited in Fig. 8.

### *2.3 Material tests*

The material properties of both the outer austenitic stainless steel circular hollow tubes and the inner high strength concrete cores of the HCFSST stub column specimens were respectively derived through tensile coupon tests and standard cylinder tests. Tensile coupons, with their geometric dimensions complying with the provisions given in EN ISO 6892-1 [24], were cut at 90 degrees from the weld of the austenitic stainless steel circular hollow tubes, and heated and cooled together with the corresponding HCFSST stub columns. Tensile coupon tests were performed through the use of a 50 kN hydraulic testing machine under displacement-control. Specifically, the initial loading speed was equal to 0.05 mm/min until the attainment of the material nominal 0.2% proof stress, and followed by an increased loading speed of 0.8 mm/mm for the post-yield stage. The tensile coupon test rig is displayed in Fig. 9, including an extensometer with the gauge length of 50 mm mounted onto the middle portion of the necked part of the coupon and a pair of strain gauges affixed to the mid-height of the coupon. For the two adopted austenitic stainless steel tube sections CHS 73×3 and CHS 89×3, the measured material stress–strain curves of the tensile coupons at room temperature and after exposure to the ISO-834 standard fire for 15 min, 30 min and 45 min are displayed in Fig. 10. The key room temperature material properties are reported in Table 2(a), including the Young's modulus $E$, the 0.2% proof stress $\sigma_{0.2}$, the ultimate stress $\sigma_u$, the strain at the ultimate stress $\varepsilon_u$, the strain at fracture $\varepsilon_f$ and the strain hardening coefficients $n$ and $m$ utilised in the Ramberg–Osgood material model [14, 25–29], while the key post-fire material properties, denoted with a subscript 'T', are summarised in Table 2(b).

High strength concretes of two grades (C90 and C140) were used for the fabrication of the HCFSST stub column specimens. The two grades of high strength concretes were produced using the CEM I 52.5N Portland cement, aggregate with the maximum size of 10 mm, river sand, fresh water, silica fume and superplasticizer, with the respective mix designs presented in Table 3. Four concrete cylinders were casted for each high strength concrete grade, with the geometric dimensions following the recommendations given in BS EN 12390-3:2009 [30], and then cured together with the HCFSST stub column specimens under the same condition of environment. Note that high strength concrete cylinders (without the confinement from the outer tube and end plates) suffer from severe explosive spalling when exposure to fire, and break apart into pieces. Therefore, standard cylinder tests can only be carried out on high strength concrete cylinders at room temperature. All the concrete cylinders were tested at a constant loading speed of 0.6 MPa/s. The average compressive strengths $f_c$ for the C90 and C140 concretes, derived from the standard cylinder tests, were respectively equal to 93.8 MPa and 144.4 MPa, with the corresponding COVs (coefficients of variation) of 0.014 and 0.007.

### *2.4 Stub column tests*

A total of 16 concentric compression tests were carried out on HCFSST stub columns to study their structural responses and residual compression resistances after exposed to fire. A 2000 kN hydraulic testing machine with fixed platens at both ends, driven by displacement-control at a constant speed of 0.3 mm/min [6, 31, 32], was adopted for all the stub column tests. Prior to the testing, both ends of the HCFSST stub column specimens were milled flat and covered with a thin layer of gypsum, which was then hardened between two flat rigid platens under a small compression load, ensuring the achievement of flat end surfaces of the specimens and thus a uniform compressive stress distribution on both the outer austenitic stainless steel circular tube and inner high strength concrete core during testing. Fig. 11 displays the stub column test setup, where a pair of stiffening rings are utilised at both ends of the specimen, to preclude any potential local failure at the specimen ends, four linear variable differential transducers (LVDTs) are employed for measuring the axial shortening of the specimen, and a pair of orthogonal strain gauges, affixed to the mid-height of the outer austenitic stainless steel circular tube of the specimen, are used to record both the longitudinal compressive strain and hoop tensile strain.

The experimentally obtained load–end shortening curves for the four specimen series are shown in Figs 12(a)–12(d), respectively. Table 4(a) summaries the measured initial compressive stiffness ($E_iA_i$), the ultimate load $N_u$ and the axial end shortening at the ultimate load $\delta_u$ for each unheated HCFSST stub column specimen; note that the initial compressive stiffness ($E_iA_i$) is defined as the product of the initial stiffness of the experimental load–end shortening curve $k$ and the specimen length $L$ (see Fig. 13). The key measured experimental results of the HCFSST stub column specimens after exposure to the ISO-834 standard fire for different durations are listed in Table 4(b), including the initial compressive stiffness $(E_iA_i)_T$, the ultimate load $N_{u,T}$, the axial end shortening at the ultimate load $\delta_{u,T}$ (the subscript 'T' signifies the post-fire test results) and the ratios of $(E_iA_i)_T/(E_iA_i)$ and $N_{u,T}/N_u$; it is worth noting that for those HCFSST stub column specimens after exposure to fire for relatively long heating durations (for example, specimen D73-C90-T45), the load–deformation responses were flat even at unrealistically large plastic deformations, and the corresponding experimental ultimate loads were given as the loads at which the tangent stiffnesses of the load–end shortening curves were equal to 1% of the initial stiffnesses [33]. Fig. 14 depicts the experimental failure modes for a typical specimen series, including the HCFSST stub column specimens D89-C90-T0, D89-C90-T15, D89-C90-T30 and D89-C90-T45, all featuring outward local buckling of the outer austenitic stainless steel tubes, along with crushing of the inner high strength concretes.

### *2.5 Discussion on post-fire HCFSST stub column test results*

#### *2.5.1 Initial compressive stiffness and ultimate compression resistance*

The effect of the heating durations on the initial compressive stiffnesses and ultimate compression resistances of HCFSST stub columns was discussed in this sub-section. The $(E_iA_i)_T/(E_iA_i)$ and $N_{u,T}/N_u$ ratios of all the four specimen series are plotted against the corresponding heating durations, and shown in Figs 15(a) and 15(b), respectively. The results of the comparison indicated that (i) both the initial compressive stiffness and the ultimate compression resistance decrease with increasing heating duration, and (ii) the initial compressive stiffness is generally more sensitive to the elevated temperature than the ultimate compression resistance. For example, with regards to the test series D89-C90, the ultimate compression resistances of the specimens after exposed to the ISO-834 standard fire for 30 min and 45 min (D89-C90-T30 and D89-C90-T45) were shown to decrease by 17.4% and 29.0%, respectively, in comparison with that of the unheated specimen (D89-C90-T0), while the corresponding initial compressive stiffnesses experienced greater decreases of 41.4% and 60.2%. Moreover, the reduction factors of the initial compressive stiffness and ultimate compression resistance are generally lower for specimen series with higher concrete grades (e.g., specimen series with concrete infill of grade C140) and more slender outer tubes (e.g., specimen series fabricated with the outer tube of CHS 89×3).

### *2.5.2 Mid-height strains of the outer austenitic stainless steel CHS tube*

The mid-height longitudinal and transverse strains of the outer austenitic stainless steel circular tubes of the HCFSST stub column specimens after exposure to fire for various heating durations were investigated in the present section. Fig. 16 depicts the load–strain curves measured from a typical specimen series D89-C90, where ‘positive’ and ‘negative’ values respectively indicate tensile and compressive strains. As can be seen from Fig. 16, the longitudinal (compressive) strains develop faster for those HCFSST stub column specimens after exposed to fire for longer heating durations, due to the greater reductions in initial compressive stiffnesses, thus leading to larger longitudinal (compressive) strains for a given compression force. The transverse (tensile) strains of the outer austenitic stainless steel tubes were also found to develop faster for those HCFSST stub column specimens after exposed to fire for longer heating durations (see Fig. 16), owing to the greater lateral expansion of the concrete infill resulted from the larger longitudinal deformation.

## 3. Numerical investigation

### *3.1 General*

Aside from the experimental study, a numerical investigation was also carried out herein by using the commercial finite element (FE) package ABAQUS [34]. Two types of FE models, namely heat transfer and mechanical FE models, were established to replicate both the experimental thermal (temperature–time) responses of the HCFSST stub column specimens during the heating and cooling process and mechanical (load–end shortening) responses of the HCFSST stub column specimens after exposure to fire. Upon validation of the heat transfer and mechanical FE models, parametric studies were performed to derive additional numerical data over a wider range of cross-section sizes.

### *3.2 Development and validation of heat transfer FE models*

The four-node heat transfer shell element DS4 [34] and eight-node heat transfer brick element DC3D8 [34] have been proved to be accurate and effective in the numerical simulation of the thermal responses of the outer thin-walled steel tubes and inner solid concrete cores of concrete-filled steel tube composite columns [22, 35, 36], and were also adopted in the present numerical modelling of the HCFSST stub column specimens during the heating and cooling process. The sizes of both the employed DC3D8 and DS4 elements were selected to be equal to $D/18$, based on a prior mesh sensitivity study considering element sizes ranging from $D/10$ to $D/30$. The thermal properties of concrete and steel, including the density, thermal conductivity and specific heat, were determined in accordance with the provisions specified in the European codes EN 1994-1-2 [37] and EN 1993-1-2 [38]; note that the lower limit model was utilised to derive the thermal conductivity of concrete, while the specific heat of concrete was revised based on the moisture content of 5% (by weight) [22]. For the HCFSST stub column specimens exposed to the ISO-834 standard fire, the heat was transmitted to the outer surfaces of the austenitic stainless steel tubes by means of convection and radiation. Modified radiative heat transfer mechanism specific for stainless steel has been proposed by Gardner and Ng [39], in which the emissivity and heat transfer coefficient are taken as 0.2 and 35 W/m$^2$K, respectively, and was also utilised herein. Owing to the distinct difference in thermal expansion properties between concrete and stainless steel, the inner concrete core and outer stainless steel tube of each HCFSST stub column specimen were not completely contacted during the heating process, resulting in a gap generated at the interface between them, and the heat transfer is allowed for through gap conductance with the coefficient taken as 100 W/m$^2$K [22, 40]. Upon development of each heat transfer HCFSST stub column FE model, the temperature–time curve measured from the surface of the austenitic stainless steel tube during the heating and cooling process, was assigned to the outer tube face of the HCFSST stub column FE model, followed by thermal analysis for the purpose of deriving the full temperature–time histories of the concrete core.

The accuracy of the established heat tranfer FE models was evaluated through comparing the numerically derived temperature–time histories of the concrete cores with the test results. Table 5 reports the experimentally and numerically obtained maximum temperatures at the three measured positions of the concrete cores for all the HCFSST stub column specimens during the heating process, indicating good agreement. Fig. 17 displays the test and FE temperature–time curves of the concrete cores at the three measured points for a typical specimen D89-C90-T45, revealing that the full ranges of the experimental (measured) temperature–time curves are well replicated by the corresponding numerical curves, To conclude, the developed heat transfer FE models are capable of predicting the test thermal responses of the HCFSST stub columns when subjected to the ISO-384 standard fire.

### *3.3 Development and validation of mechanical FE models*

Mechanical FE models were developed to replicate the structural responses of the HCFSST stub column specimens after exposure to fire in this section. The eight-node brick element

C3D8R [34] and four-node shell element S4R [34] were utilised in the present numerical modelling of the inner solid concrete cores and outer thin-walled stainless steel tubes, with the element sizes of $D/18$ (i.e. identical to those utilised in the heat transfer FE models). With regards to the material modelling of austenitic stainless steel tubes at room temperature and after exposure to fire, the room temperature and post-fire material stress–strain curves derived from the material testing were firstly converted into the true stress–true plastic strain curves, and then inputted into the plastic material model provided in ABAQUS. The concrete damage plasticity (CDP) model [34] was adopted to represent the material stress–strain responses of high strength concrete at room temperature and after exposed to fire. Specifically, for concrete at room temperature, the elastic modulus and Poisson's ratio were taken as $4700\sqrt{f_c}$ and 0.2 [41], respectively, while the plastic parameters used in the CDP model were calculated in accordance with the recommendations given in Tao et al. [42]. For concrete after exposure to fire, the residual compressive strength $f_{c,T}$ (the subscript 'T' indicates the post-fire residual material property) and strain at the residual compressive strength $\varepsilon_{c,T}$ were determined from Eqs (1) and (2) [36, 43, 44], in which $f_c$ and $\varepsilon_c$ are respectively the concrete compressive strength and the corresponding compressive strain at room temperature and $T_{max}$ is the maximum attained temperature of the concrete during the heating process, while other material parameters in the CDP model, depending on $f_{c,T}$ and $\varepsilon_{c,T}$, can then be derived accordingly. To consider the beneficial effect of confinement provided by the outer austenitic stainless steel circular tube to the inner high strength concrete core, equivalent uniaxial compressive stress–strain responses, derived from the confined concrete model proposed by Tao et al. [42], were inputted into the CDP model. The tensile stress–strain relationship of concrete is assumed to be linear and elastic up to the concrete tensile strength of $0.1f_c$ (or $0.1f_{c,T}$), followed by an inelastic post-ultimate material response, characterised by means of fracture energy ($G_F$) [45]. It is worth noting that the maximum attained temperatures of the inner concrete core of the

HCFSST stub column specimen exposed to the ISO-384 standard fire vary along the radial direction, leading to different post-fire material stress–strain responses for different layers of the inner concrete core. In the present numerical modelling, the inner concrete core is discretised into layers according to the mesh size, and the maximum temperature of each layer was extracted from the prior heat transfer analysis and used to derive the post-fire material stress–strain response.

$$f_{c,T} = f_c / [1 + 2.4\left(T_{\max} - 20\right)^6 \times 10^{-17}] \tag{1}$$

$$\varepsilon_{c,T} = \varepsilon_c \times [1 + (1500T_{\max} + 5T_{\max}^2) \times 10^{-6}] \tag{2}$$

The interaction between the inner high strength concrete core and outer austenitic stainless steel circular tube was simulated by means of the surface-to-surface contact [18, 42, 46, 47]. The inner surface of the thin-walled austenitic stainless steel circular tube and the outer surface of the solid concrete core were respectively selected as the ‘slave surface’ and ‘master surface’. The contact behaviour between the two interfaces in the normal direction was represented by a hard contact pressure–overclosure relationship, while a penalty method was adopted to define the tangential behaviour between the two interfaces. Given that there have been no well-established friction coefficients for the modelling of the post-fire tangential behaviour between stainless steel tube and concrete infill, a sensitivity study was performed to seek the most suitable value of the friction coefficient. It was generally found that the post-fire mechanical responses of HCFSST stub columns were insensitive to the amplitudes of the friction coefficient. Therefore, the friction coefficient of 0.25, extensively used in the numerical simulations of concrete-filled steel tube stub columns at room temperature [46], was adopted throughout the present numerical modelling. Moreover, all degrees of freedom of the two end sections of each HCFSST stub column FE model were restrained except for the translation in the longitudinal direction at one end, allowing for the achievement of the same fixed-ended boundary condition as that used in the tests.

Upon development of the mechanical HCFSST stub column FE models, nonlinear analysis was carried out to derive the numerical ultimate loads, load–deformation histories and deformed failure modes, which were then compared with the corresponding experimental results, allowing the accuracy of the developed mechanical FE models to be evaluated. Table 4 presents the ratios of FE to experimental failure loads for the HCFSST stub column specimens, indicating that the developed mechanical FE models yield a high degree of accuracy and consistency in predicting the experimental ultimate loads. The FE load–end shortening curves for a typical specimen series D89-C90 are displayed in Fig. 18, together with their experimental counterparts, where the initial stiffnesses, failure loads and general shapes of the test load–deformation responses are found to be well captured by numerical modelling. Comparisons between the test and numerical failure modes for a typical specimen series D89-C90 are illustrated in Fig. 14, also indicating good agreement. Overall, the developed mechanical FE models are capable of precisely simulating the post-fire structural responses of the HCFSST stub column specimens, and thus deemed to be validated.

### *3.4 Numerical parametric studies*

On the basis of the validated heat transfer and mechanical FE models, parametric studies were performed herein to generate additional numerical data on HCFSST stub columns over a wider range of cross-section sizes. In the present parametric studies, the measured room temperature and post-fire material properties of the austenitic stainless steel circular hollow section CHS 89×3 were adopted for the outer tubes of the modelled HCFSST stub columns, while high strength concretes of two grades C90 and C140 with the corresponding measured cylinder strengths at room temperature equal to 93.8 MPa and 144.4 MPa were utilised for the inner concrete cores. In terms of the cross-section dimensions, the outer diameters of the modelled austenitic stainless steel circular tubes were respectively equal to 100 mm, 125 mm and 150 mm, with the outer diameter-to-thickness ratios varied between 20 and 50. The developed HCFSST stub column FE models were exposed to the ISO-384 standard fire for three heating durations of 15 min, 30 min and 45 min. A summary of the geometric dimensions, material grades and heating durations selected for parametric studies is shown in Fig. 19. A total of 72 numerical data on HCFSST stub columns after exposure to fire were generated in the present parametric studies.

## 4. Evaluation of current design standards

### *4.1 General*

Due to the absence of established design standards for concrete-filled stainless steel tube members and concrete-filled carbon steel tube members after exposure to fire, the corresponding codified design provisions for circular concrete-filled carbon steel tube members at room temperature, as set out in the European code EN 1994-1-1 [11], Australian Standard AS 5100 [12] and American Specifications AISC 360 [13], were evaluated for their suitability to circular HCFSST stub columns after exposure to fire, based on the derived test and numerical results. In the present evaluation, the inner concrete core of each HCFSST stub column was discretised into five layers, with the respective maximum attained temperatures at the mid-points of the layers extracted from the numerical heat transfer analysis, to account for the uneven temperature field along the radial direction, and the post-fire residual compressive strength of each concrete layer $f_{c,T}$ was then obtained from Eq. (3), where $T_{max}$ is the maximum attained temperature at the mid-point of the considered concrete layer, and $k_{c,T_{\max}}$ is the strength reduction factor and can be derived from Table 3.3 of EN 1994-1-2 [37]. The final design residual compressive strength of the whole concrete section $f_{c,w,T}$ was given as the weighted average (by area) residual compressive strength from all the five layers. Note that the current Australian and American specifications provide no formulations for calculating the compressive strength of concrete after exposure to fire, and thus Eq. (3), as specified in the European code EN 1994-1-2 [37], was adopted to determine the post-fire material strength of concrete throughout the present evaluation. Table 6 presents the mean ratios of the test and FE ultimate loads to the (unfactored) predicted ultimate loads $N_{u,T}/N_{u,T,pred}$ for all the three considered design standards.

$$f_{c,T} = f_c \begin{cases} k_{c,T_{\max}} & 20\,°\mathrm{C} \le T_{\max} < 100\,°\mathrm{C} \\ 1.0 - [0.235 \times (T_{\max} - 100)/200] & 100\,°\mathrm{C} \le T_{\max} < 300\,°\mathrm{C} \\ 0.9 k_{c,T_{\max}} & T_{\max} > 300\,°\mathrm{C} \end{cases} \tag{3}$$

### *4.2 European code EN 1994-1-1 (EC4)*

The compression resistances of circular concrete-filled carbon steel tube columns at room temperature, as specified in the current European code EN 1994-1-1 [11], were determined by Eq. (4),

$$N_{u,EC4} = \eta_a A_s f_y + A_c f_c \left(1 + \eta_c \frac{t}{D}\frac{f_y}{f_c}\right) \tag{4}$$

where $\eta_c$ is an enhancement factor, accounting for the beneficial effect of confinement (provided by the outer circular tube to the inner concrete core) on the compressive strength of concrete, as calculated from Eq. (5), and $\eta_a$ is a reduction factor, considering the loss of material strength of the outer steel tube in the longitudinal (loading) direction due to the development of tensile hoop stress to confine the inner concrete core, as derived by Eq. (6),

$$\eta_c = 4.9 - 18.5\bar{\lambda} + 17\bar{\lambda}^2 \geq 0 \tag{5}$$

$$\eta_a = 0.25(3 + 2\bar{\lambda}) \leq 1.0 \tag{6}$$

in which $\bar{\lambda}$ is the relative member slenderness and can be obtained by using Eq. (7), where $N_{pl,Rk}$ is the plastic resistance of the composite cross-section and calculated from Eq. (8), and $N_{cr}$ is the elastic critical normal force, as calculated from Eq. (9),

$$\bar{\lambda} = \sqrt{\frac{N_{pl,Rk}}{N_{cr}}} \tag{7}$$

$$N_{pl,Rk} = A_s f_y + A_c f_c \tag{8}$$

$$N_{cr} = \frac{\pi^2 (EI)_{eff}}{(0.5L)^2} \tag{9}$$

in which $(EI)_{eff}$ is the effective flexural stiffness and derived by Eq. (10), where $E_s$ and $E_{cm}$ are respectively the elastic moduli of the outer steel tube and inner concrete core, and $I_s$ and $I_c$ are the second moments of area of the outer steel tube and inner concrete core.

$$(EI)_{eff} = E_s I_s + 0.6 E_{cm} I_c \tag{10}$$

The compression resistances of the studied HCFSST stub columns after exposure to fire were calculated herein by using Eqs (4)–(10), but with $f_y=\sigma_{0.2,T}$ and $f_c=f_{c,w,T}$, in which $\sigma_{0.2,T}$ is the post-fire material 0.2% proof stress of the outer austenitic stainless steel tube, as given in Table 2, while $f_{c,w,T}$ is the weighted average residual compressive strength of the inner concrete core. The mean experimental (and numerical) to EC4 predicted cross-section compressive resistance ratio $N_{u,T}/N_{u,T,EC4}$ and the corresponding COV, as listed in Table 6, are equal to 1.18 and 0.09, respectively, revealing that the EC4 design provisions for circular concrete-filled carbon steel tube stub columns at room temperature can be safely applied to circular high strength concrete-filled stainless steel tube (HCFSST) stub columns after exposure to fire, with a high level of accuracy and consistency in predicting the post-fire residual compression resistances. Good agreement between the experimental (and numerical) and EC4 predicted resistances is also shown in Fig. 20, in which the ratios of $N_{u,T}/N_{u,T,EC4}$ are plotted against the $D/t$ ratios of the outer austenitic stainless steel circular hollow tubes of the HCFSST stub column specimens.

### *4.3 Australian standard AS 5100*

The current Australian Standard AS 5100 [12] adopts the same design formulations for determining the design compression resistances of circular concrete-filled carbon steel tube columns as those set out in the European code EN 1994-1-1 [11], except for the use of an alternative expression for relative member slenderness, as given in Eq. (11). The suitability of AS 5100 [12] to the design of HCFSST stub columns after exposure to fire was evaluated through comparing the AS design compression resistances with the experimental and numerical ultimate resistances. The AS design compression resistances were determined from Eqs (4)–(9) and Eq. (11), but with the post-fire stainless steel and concrete material strengths replacing their room temperature counterparts. As reported in Table 6, the mean ratio of $N_{u,T}/N_{u,T,AS}$ is equal to 1.20, with the corresponding COV of 0.10. The results of the assessment revealed that the AS design provisions for circular concrete-filled carbon steel tube stub columns at room temperature can be safely applied to circular HCFSST stub columns after exposed to fire, with a good level of design accuracy and consistency, as also evident in Fig. 21.

$$(EI)_{eff} = E_s I_s + E_{cm} I_c \tag{11}$$

### 4.4 American specification AISC 360

The design cross-section compression resistances of circular concrete-filled carbon steel tube stub columns, as specified in AISC 360 [13], are dependent on the classes of the outer carbon steel tube sections. Three classes of circular hollow sections with concrete infill, namely compact sections, non-compact sections and slender sections, are defined through comparing the outer diameter-to-thickness ratio $\lambda=D/t$ of the section against the limiting slendernesses, respectively taken as $\lambda_p = 0.15E / f_y$ and $\lambda_p = 0.19E / f_y$ for compact/non-compact sections and non-compact/slender sections. With regards to compact CHS with concrete infill (i.e. $\lambda<\lambda_p$), the outer CHS is capable of achieving the material yield strength $f_y$ at failure and also providing sufficient confinement to the concrete infill to achieve its effective compressive strength of $0.95f_c$, leading to the formulation for the calculation of cross-section compression resistance given in Eq. (12). Non-compact CHS with $\lambda_p\leq\lambda<\lambda_r$ is still assumed to attain the material yield stress at failure, but cannot offer sufficient confinement to enable the concrete infill to reach the effective compressive strength, with the design expression for compression resistances of non-compact circular concrete-filled carbon steel tube section stub columns given in Eq. (13). Slender circular hollow tube sections with $\lambda\geq\lambda_r$ suffer from local buckling prior to the achievement of the material yield stress at failure, and are also unable to provide efficient confinement to the inner concrete cores; this respectively limits the design stresses of the steel tubes and concrete cores to the elastic critical local buckling stress $f_{cr}$ and $0.7f_c$, leading to Eq. (14) for cross-section resistances of slender circular concrete-filled carbon steel tube section stub columns.

$$N_{u,AISC} = f_y A_s + 0.95 f_c A_c \quad \text{for } \lambda < \lambda_p \tag{12}$$

$$N_{u,AISC} = f_y A_s + 0.95 f_c A_c - \frac{0.25 f_c A_c}{(\lambda_r - \lambda_p)^2}(\lambda - \lambda_p)^2 \quad \text{for } \lambda_p \leq \lambda < \lambda_r \tag{13}$$

$$N_{u,AISC} = f_{cr} A_s + 0.7 f_c A_c \quad \text{for } \lambda \geq \lambda_r \tag{14}$$

The applicability of the AISC 360-16 design rules to HCFSST stub columns after exposure to fire was evaluated by comparing the predicted compression resistances against the test and FE results. The AISC post-fire compression resistances of HCFSST stub columns were calculated herein by Eqs (12)–(14), but with the room temperature material properties replaced by the corresponding post-fire material characteristics. The mean test (or numerical) to AISC predicted resistance ratio $N_{u,T}/N_{u,T,AISC}$ is equal to 1.52, with the corresponding COV of 0.14, as listed in Table 6, indicating that the AISC design provisions for circular concrete-filled carbon steel tube stub columns at room temperature yield safe but rather conservative and scattered compression resistances for circular HCFSST stub columns after exposure to fire, as can also be seen from Fig. 22.

Evaluation of the applicability of the three established standards to the design of circular HCFSST stub columns after exposure to fire was also performed based on the test data only, with the experimental to predicted failure load ratios for each design standard listed in Table 7. Both of the European code and Australian standard were generally shown to result in precise design residual compression capacities for the circular HCFSST stub column specimens after exposure to fire, while the American specification yields unduly conservative capacity predictions.

## 5. Conclusions

A comprehensive experimental and numerical investigation has been performed in this paper to study the post-fire structural responses and residual compression capacities of circular high strength concrete-filled stainless steel tube (HCFSST) stub columns. The experimental investigation was conducted on 12 circular HCFSST stub column specimens after exposure to the ISO-834 standard fire, with three heating durations of 15 min, 30 min and 45 min considered, and 4 unheated reference specimens. Based on the experimental observations, it was generally found that (i) both the initial compressive stiffnesses and ultimate compression resistances of the HCFSST stub column specimens decrease with increasing heating durations, and the initial compressive stiffnesses are also more sensitive to elevated temperatures than the ultimate compression resistances and (ii) both the longitudinal (compressive) strains and transverse (tensile) strains of the outer austenitic stainless steel tubes develop faster for the HCFSST stub column specimens after exposure to fire for longer heating durations. The experimental investigation was followed by a numerical modelling study, where both heat transfer and mechanical FE models were developed to respectively simulate the thermal and mechanical responses of the circular HCFSST stub column specimens after exposure to fire, and then adopted to conduct parametric studies to expand the experimental data pool over a broader range of cross-section sizes. Due to the absence of established design codes for concrete-filled stainless steel tube members and concrete-filled carbon steel tube members after exposure to fire, the corresponding design provisions for circular concrete-filled carbon steel tube columns at room temperature, as given in EN 1994-1-1 [11], AS 5100 [12] and AISC 360 [13], were assessed for their applicability to circular HCFSST stub columns after exposure to fire, based on the test and numerical results. The results of the assessment indicated that EN 1994-1-1 [11] and AS 5100 [12] lead to a high level of accuracy and consistency in the prediction of post-fire compression resistances of circular HCFSST stub columns, while AISC 360 [13] results in rather conservative and scattered resistance predictions.

## Acknowledgements

The authors are grateful to Mr. Subasanran Chelladurai, Mr. Cheng Hoon Tui and Mr. Jason Hutomo Aryanto for their assistances during testing. The research work described in this paper is financially support by the Academic Research Fund (AcRF) Tier 1 Grant (Project ID: 2018-T1-001-243) from the Ministry of Education, Singapore.

## References

[1] Han L-H, Xu C-Y, Tao Z. Performance of concrete filled stainless steel tubular (CFSST) columns and joints: Summary of recent research. Journal of Constructional Steel Research. 2019;152:117-31.

[2] Uy B, Tao Z, Han LH. Behaviour of short and slender concrete-filled stainless steel tubular columns. Journal Of Constructional Steel Research. 2011;67:360-78.

[3] Lam D, Gardner L. Structural design of stainless steel concrete filled columns. Journal of Constructional Steel Research. 2008;64:1275-82.

[4] Yang Y-F, Ma G-L. Experimental behaviour of recycled aggregate concrete filled stainless steel tube stub columns and beams. Thin-Walled Structures. 2013;66:62-75.

[5] Li YL, Zhao XL, Singh RKR, Al-Saadi S. Experimental study on seawater and sea sand concrete filled GFRP and stainless steel tubular stub columns. Thin-Walled Structures. 2016;106:390-406.

[6] Liao F-Y, Hou C, Zhang W-J, Ren J. Experimental investigation on sea sand concrete-filled stainless steel tubular stub columns. Journal of Constructional Steel Research. 2019;155:46-61.

[7] Yang Y-F, Hou C, Liu M. Experimental Study and Numerical Analysis of CFSST Columns Subjected to Lateral Cyclic Loading. Journal of Structural Engineering. 2018;144.

[8] Liao F-Y, Han L-H, Tao Z, Rasmussen KJR. Experimental Behavior of Concrete-Filled Stainless Steel Tubular Columns under Cyclic Lateral Loading. Journal of Structural Engineering. 2017;143.

[9] Han L-H, Chen F, Liao F-Y, Tao Z, Uy B. Fire performance of concrete filled stainless steel tubular columns. Engineering Structures. 2013;56:165-81.

[10] Tao Z, Ghannam M, Song T-Y, Han L-H. Experimental and numerical investigation of concrete-filled stainless steel columns exposed to fire. Journal of Constructional Steel Research. 2016;118:120-34.

[11] EN 1994-1-1:2004. Eurocode 4: design of composite steel and concrete structures – Part 1-1: General rules and rules for buildings. Brussels: European Committee for Standardization (CEN); 2004.

[12] Standards Australia. Bridge design, Part 6: steel and composite construction. AS5100.6-2004, Sydney, Australia; 2004.

[13] American Institute of Steel Construction (AISC). Specification for structural steel buildings. AISC 360-16, Chicago (IL); 2016.

[14] He A, Liang Y, Zhao O. Experimental and numerical studies of austenitic stainless steel CHS stub columns after exposed to elevated temperatures. Journal of Constructional Steel Research. 2019;154:293-305.

[15] Zhao O, Gardner L, Young B. Structural performance of stainless steel circular hollow sections under combined axial load and bending – Part 1: Experiments and numerical modelling. Thin-Walled Structures. 2016;101:231-9.

[16] Zhao O, Gardner L, Young B. Structural performance of stainless steel circular hollow sections under combined axial load and bending – Part 2: Parametric studies and design. Thin-Walled Structures. 2016;101:240-8.

[17] Zhao O, Gardner L, Young B. Testing and numerical modelling of austenitic stainless steel CHS beam–columns. Engineering Structures. 2016;111:263-74.

[18] He A, Zhao O. Experimental and numerical investigations of concrete-filled stainless steel tube stub columns under axial partial compression. Journal of Constructional Steel Research. 2019;158:405-16.

[19] ISO-834. Fire resistance tests—elements of building construction. Switzerland: International Organization for Standardization; 1975.

[20] Liu J-C, Tan KH, Yao Y. A new perspective on nature of fire-induced spalling in concrete. Construction and Building Materials. 2018;184:581-90.

[21] Huo J, Huang G, Xiao Y. Effects of sustained axial load and cooling phase on post-fire behaviour of concrete-filled steel tubular stub columns. Journal of Constructional Steel Research. 2009;65:1664-76.

[22] Liu F, Gardner L, Yang H. Post-fire behaviour of reinforced concrete stub columns confined by circular steel tubes. Journal of Constructional Steel Research. 2014;102:82-103.

[23] Annerel E, Taerwe L. Revealing the temperature history in concrete after fire exposure by microscopic analysis. Cement and Concrete Research. 2009;39:1239-49.

[24] EN ISO 6892-1. Metallic materials – tensile testing – Part 1: Method of test at room temperature. Brussels: European Committee for Standardization (CEN); 2009.

[25] Ramberg W, Osgood WR. Description of stress–strain curves by three parameters. Technical note no. 902. Washington DC: National Advisory Committee for Aeronautics; 1943.

[26] Hill HN. Determination of stress–strain relations from offset yield strength values. Technical note no. 927. Washington DC: National Advisory Committee for Aeronautics; 1944.

[27] Mirambell E, Real E. On the calculation of deflections in structural stainless steel beams: an experimental and numerical investigation. Journal of Constructional Steel Research. 2000;54:109-33.

[28] Rasmussen KJR. Full-range stress–strain curves for stainless steel alloys. Journal of Constructional Steel Research. 2003;59:47-61.

[29] Gardner L, Ashraf M. Structural design for non-linear metallic materials. Engineering Structures. 2006;28:926-34.

[30] EN 12390-3:2009. Testing hardened concrete – Part 3: Compressive strength of test specimens. Brussels: European Committee for Standardization (CEN); 2009.

[31] Tao Z, Song T-Y, Uy B, Han L-H. Bond behavior in concrete-filled steel tubes. Journal of Constructional Steel Research. 2016;120:81-93.

[32] Wang F, Young B, Gardner L. Compressive testing and numerical modelling of concrete-filled double skin CHS with austenitic stainless steel outer tubes. Thin-Walled Structures. 2019;141:345-59.

[33] dos Santos GB, Gardner L, Kucukler M. A method for the numerical derivation of plastic collapse loads. Thin-Walled Structures. 2018;124:258-77.

[34] ABAQUS. ABAQUS/standard user's manual volumes I–III and ABAQUS CAE manual. Version 6.12. Pawtucket (USA): Hibbitt, Karlsson & Sorensen, Inc; 2012.

[35] Tao Z, Ghannam M. Heat transfer in concrete-filled carbon and stainless steel tubes exposed to fire. Fire Safety Journal. 2013;61:1-11.

[36] Song T-Y, Han L-H, Yu H-X. Concrete filled steel tube stub columns under combined temperature and loading. Journal of Constructional Steel Research. 2010;66:369-84.

[37] EN 1994-1-2:2005+A1:2014. Eurocode 4: design of composite steel and concrete structures – Part 1-2: General rules — Structural fire design. Brussels: European Committee for Standardization (CEN); 2014.

[38] EN 1993-1-2:2005. Eurocode 3: Design of steel structures – Part 1-2: General rules — Structural fire design. Brussels: European Committee for Standardization (CEN); 2005.

[39] Gardner L, Ng KT. Temperature development in structural stainless steel sections exposed to fire. Fire Safety Journal. 2006;41:185-203.

[40] Lu H, Zhao X-L, Han L-H. FE modelling and fire resistance design of concrete filled double skin tubular columns. Journal of Constructional Steel Research. 2011;67:1733-48.

[41] American Concrete Institute. Building code requirements for structural concrete. ACI 318-14, Farmington Hills, MI; 2014.

[42] Tao Z, Wang Z-B, Yu Q. Finite element modelling of concrete-filled steel stub columns under axial compression. Journal of Constructional Steel Research. 2013;89:121-31.

[43] Han LH. Concrete filled steel tubular structures (second version). Beijing: China Science Press; 2007 [in Chinese].

[44] Yang H, Han L-H, Wang Y-C. Effects of heating and loading histories on post-fire cooling behaviour of concrete-filled steel tubular columns. Journal of Constructional Steel Research. 2008;64:556-70.

[45] CEB-FIP (Euro-International Committee for Concrete (CEB)-International Federation for Prestressing (FIP).). Model Code for concrete structures. (CEB-FIP MC 2010). London, U.K.: Thomas Telford; 2010.

[46] Tao Z, Uy B, Liao F-Y, Han L-H. Nonlinear analysis of concrete-filled square stainless steel stub columns under axial compression. Journal of Constructional Steel Research. 2011;67:1719-32.

[47] He A, Wang F, Zhao O. Experimental and numerical studies of concrete-filled high-chromium stainless steel tube (CFHSST) stub columns. Thin-Walled Structures. 2019; 144:106273.

**Table 1** Measured geometric dimensions and maximum attained temperatures of HCFSST stub column specimens.

| Specimen | $D$ (mm) | $t$ (mm) | $L$ (mm) | $T_h$ (min) | $T_1$ (°C) | $T_2$ (°C) | $T_3$ (°C) | $T_4$ (°C) |
|---|---|---|---|---|---|---|---|---|
| D73-C90-T0 | 72.8 | 2.81 | 216 | 0 | - | - | - | - |
| D73-C90-T15 | 73.1 | 2.79 | 215 | 15 | 326 | 324 | 325 | 687 |
| D73-C90-T30 | 73.1 | 2.83 | 216 | 30 | 616 | 581 | 579 | 817 |
| D73-C90-T45 | 72.7 | 2.83 | 215 | 45 | 849 | 789 | 787 | 881 |
| D73-C140-T0 | 72.8 | 2.80 | 217 | 0 | - | - | - | - |
| D73-C140-T15 | 72.7 | 2.80 | 216 | 15 | 411 | 413 | -* | 687 |
| D73-C140-T30 | 72.8 | 2.80 | 221 | 30 | 626 | -* | 623 | 817 |
| D73-C140-T45 | 72.6 | 2.82 | 216 | 45 | 849 | 789 | 787 | 881 |
| D89-C90-T0 | 89.3 | 2.82 | 267 | 0 | - | - | - | - |
| D89-C90-T15 | 88.9 | 2.83 | 270 | 15 | 301 | 297 | 297 | 687 |
| D89-C90-T30 | 88.6 | 2.79 | 268 | 30 | 567 | 522 | 524 | 817 |
| D89-C90-T45 | 88.9 | 2.79 | 266 | 45 | 824 | 720 | 709 | 881 |
| D89-C140-T0 | 89.3 | 2.83 | 267 | 0 | - | - | - | - |
| D89-C140-T15 | 88.9 | 2.82 | 270 | 15 | 290 | 288 | 288 | 687 |
| D89-C140-T30 | 89.3 | 2.84 | 268 | 30 | 687 | 675 | 666 | 817 |
| D89-C140-T45 | 88.9 | 2.77 | 268 | 45 | 820 | -* | 696 | 881 |

* The thermocouples were damaged during the fabrication of the HCFSST stub column specimens and their values were not obtained.

**Table 2** Measured key material properties from tensile coupon tests.

(a) At room temperature

| Cross-section | $T$ (°C) | $E$ (GPa) | $\sigma_{0.2}$ (MPa) | $\sigma_u$ (MPa) | $\varepsilon_u$ (%) | $\varepsilon_f$ (%) | $n$ | $m$ |
|---|---|---|---|---|---|---|---|---|
| CHS 73×3 | 30 | 206 | 296 | 715 | 50 | 58 | 5.5 | 2.5 |
| CHS 89×3 | 30 | 202 | 292 | 727 | 55 | 66 | 4.1 | 2.4 |

(b) After exposure to the ISO-834 standard fire for three levels of heating durations

| Cross-section | $T_h$ (min) | $T_4$ (°C) | $E_T$ (GPa) | $\sigma_{0.2,T}$ (MPa) | $\sigma_{u,T}$ (MPa) | $\varepsilon_{u,T}$ (%) | $\varepsilon_{f,T}$ (%) | $n_T$ | $m_T$ |
|---|---|---|---|---|---|---|---|---|---|
| CHS 73×3 | 15 | 687 | 205 | 289 | 706 | 52 | 62 | 6.7 | 2.4 |
| | 30 | 817 | 202 | 275 | 701 | 59 | 72 | 6.5 | 2.4 |
| | 45 | 881 | 208 | 261 | 703 | 51 | 60 | 7.0 | 2.3 |
| CHS 89×3 | 15 | 687 | 202 | 284 | 692 | 59 | 72 | 6.2 | 2.4 |
| | 30 | 817 | 195 | 275 | 686 | 48 | 58 | 5.7 | 2.4 |
| | 45 | 881 | 194 | 283 | 698 | 58 | 77 | 5.2 | 2.4 |

**Table 3** Mixture proportion of concretes.

| Grade | Gravel (kg) | Sand (kg) | Cement (kg) | Water (kg) | Silica fume (kg) | Superplasticizer (kg) |
|---|---|---|---|---|---|---|
| C90 | 736 | 746 | 457 | 189 | 67 | 5 |
| C140 | 977 | 652 | 637 | 141 | 100 | 10 |

**Table 4** Summary of experimental and numerical results on HCFSST stub columns at room temperature and after exposure to fire.

(a) At room temperature

| Specimen | $(E_iA_i)$ ($\times10^4$ kN) | $N_u$ (kN) | $\delta_u$ (mm) | $N_{u,FE}$ (kN) | $N_{u,FE}/N_u$ |
|---|---|---|---|---|---|
| D73-C90-T0 | 25.98 | 561 | 1.76 | 575 | 1.02 |
| D73-C140-T0 | 31.13 | 739 | 1.26 | 715 | 0.97 |
| D89-C90-T0 | 40.59 | 924 | 1.97 | 815 | 0.88 |
| D89-C140-T0 | 44.53 | 1072 | 1.22 | 1040 | 0.97 |

(b) After exposure to fire

| Specimen | $(E_iA_i)_T$ ($\times10^4$kN) | $N_{u,T}$ (kN) | $\delta_{u,T}$ (mm) | $(E_iA_i)_T/(E_iA_i)$ | $N_{u,T}/N_u$ | $N_{u,T,FE}$ (kN) | $N_{u,T,FE}/N_{u,T}$ |
|---|---|---|---|---|---|---|---|
| D73-C90-T15 | 17.91 | 554 | 3.29 | 0.69 | 0.99 | 600 | 1.08 |
| D73-C90-T30 | 13.52 | 596 | 8.28 | 0.52 | 1.06 | 452 | 0.76 |
| D73-C90-T45 | 13.22 | 485 | 11.73 | 0.51 | 0.87 | 543 | 1.12 |
| D73-C140-T15 | 20.02 | 792 | 2.03 | 0.64 | 1.07 | 759 | 0.96 |
| D73-C140-T30 | 14.22 | 624 | 5.03 | 0.46 | 0.84 | 515 | 0.83 |
| D73-C140-T45 | 13.78 | 501 | 6.64 | 0.44 | 0.68 | 517 | 1.03 |
| D89-C90-T15 | 29.70 | 836 | 2.15 | 0.73 | 0.90 | 821 | 0.98 |
| D89-C90-T30 | 23.80 | 763 | 6.79 | 0.59 | 0.83 | 664 | 0.87 |
| D89-C90-T45 | 16.15 | 656 | 11.13 | 0.40 | 0.71 | 618 | 0.94 |
| D89-C140-T15 | 33.02 | 816 | 2.91 | 0.74 | 0.76 | 1061 | 1.30 |
| D89-C140-T30 | 20.21 | 777 | 6.85 | 0.45 | 0.72 | 796 | 1.02 |
| D89-C140-T45 | 17.10 | 641 | 13.69 | 0.38 | 0.60 | 664 | 1.04 |

**Table 5** Comparison of test and numerical maximum attained temperatures.

| Specimen | $T_1$ (°C) | $T_2$ (°C) | $T_3$ (°C) | $T_{1,FE}$ (°C) | $T_{2,FE}$ (°C) | $T_{3,FE}$ (°C) | $T_{1,FE}/T_1$ | $T_{2,FE}/T_2$ | $T_{3,FE}/T_3$ |
|---|---|---|---|---|---|---|---|---|---|
| D73-C90-T15 | 326 | 324 | 325 | 409 | 366 | 364 | 1.26 | 1.13 | 1.12 |
| D73-C90-T30 | 616 | 581 | 579 | 701 | 638 | 635 | 1.14 | 1.10 | 1.10 |
| D73-C90-T45 | 849 | 789 | 787 | 821 | 771 | 768 | 1.03 | 1.00 | 0.99 |
| D73-C140-T15 | 411 | 413 | -* | 409 | 366 | 364 | 1.00 | 0.89 | - |
| D73-C140-T30 | 626 | -* | 623 | 701 | 638 | 635 | 1.12 | - | 1.02 |
| D73-C140-T45 | 849 | 789 | 787 | 821 | 771 | 768 | 0.97 | 0.98 | 0.98 |
| D89-C90-T15 | 301 | 297 | 297 | 376 | 315 | 314 | 1.25 | 1.06 | 1.05 |
| D89-C90-T30 | 567 | 522 | 524 | 647 | 565 | 562 | 1.14 | 1.08 | 1.07 |
| D89-C90-T45 | 824 | 720 | 709 | 776 | 703 | 700 | 0.94 | 0.98 | 0.99 |
| D89-C140-T15 | 290 | 288 | 288 | 376 | 315 | 314 | 1.30 | 1.09 | 1.09 |
| D89-C140-T30 | 687 | 675 | 666 | 647 | 565 | 562 | 0.94 | 0.84 | 0.84 |
| D89-C140-T45 | 820 | -* | 696 | 776 | 703 | 700 | 0.95 | - | 1.01 |
| | | | | | | Mean | 1.09 | 1.02 | 1.02 |
| | | | | | | COV | 0.12 | 0.09 | 0.08 |

* The thermocouples were damaged during the fabrication of the HCFSST stub column specimens and their values were not obtained.

**Table 6** Comparison of test and numerical results with predicted resistances.

| No. of tests:16<br>No. of FE simulations: 72 | EC4 [11]<br>$N_{u,T}/N_{u,T,EC4}$ | AS 5100 [12]<br>$N_{u,T}/N_{u,T,AS}$ | AISC 360 [13]<br>$N_{u,T}/N_{u,T,AISC}$ |
|---|---|---|---|
| Mean value | 1.18 | 1.20 | 1.52 |
| COV | 0.09 | 0.10 | 0.14 |

**Table 7** Comparison of test results with predicted resistances.

| Specimen | Test | EC4 [11] | | AS 5100 [12] | | AISC 360 [13] | |
|---|---|---|---|---|---|---|---|
| | $N_{u,T}$ (kN) | $N_{u,T,EC4}$ (kN) | $N_{u,T}/N_{u,T,EC4}$ | $N_{u,T,AS}$ (kN) | $N_{u,T}/N_{u,T,AS}$ | $N_{u,T,AISC}$ (kN) | $N_{u,T}/N_{u,T,AISC}$ |
| D73-C90-T0 | 561 | 612 | 0.92 | 600 | 0.93 | 492 | 1.14 |
| D73-C90-T15 | 554 | 526 | 1.05 | 515 | 1.08 | 406 | 1.36 |
| D73-C90-T30 | 596 | 398 | 1.50 | 387 | 1.54 | 279 | 2.14 |
| D73-C90-T45 | 485 | 317 | 1.53 | 307 | 1.58 | 208 | 2.33 |
| D73-C140-T0 | 739 | 784 | 0.94 | 773 | 0.95 | 661 | 1.12 |
| D73-C140-T15 | 792 | 646 | 1.23 | 635 | 1.25 | 524 | 1.51 |
| D73-C140-T30 | 624 | 447 | 1.40 | 435 | 1.43 | 330 | 1.89 |
| D73-C140-T45 | 501 | 341 | 1.47 | 331 | 1.51 | 233 | 2.15 |
| D89-C90-T0 | 924 | 876 | 1.06 | 862 | 1.07 | 715 | 1.29 |
| D89-C90-T15 | 836 | 736 | 1.14 | 721 | 1.16 | 584 | 1.43 |
| D89-C90-T30 | 763 | 547 | 1.40 | 533 | 1.43 | 403 | 1.89 |
| D89-C90-T45 | 656 | 470 | 1.40 | 456 | 1.44 | 323 | 2.03 |
| D89-C140-T0 | 1072 | 1147 | 0.93 | 1133 | 0.95 | 979 | 1.10 |
| D89-C140-T15 | 816 | 936 | 0.87 | 923 | 0.88 | 781 | 1.05 |
| D89-C140-T30 | 777 | 667 | 1.16 | 654 | 1.19 | 518 | 1.50 |
| D89-C140-T45 | 641 | 527 | 1.22 | 513 | 1.25 | 380 | 1.68 |
| | | Mean | 1.20 | | 1.23 | | 1.60 |
| | | COV | 0.19 | | 0.19 | | 0.26 |


(a) Inside view

(b) Outside review

**Fig. 1.** Electric furnace.

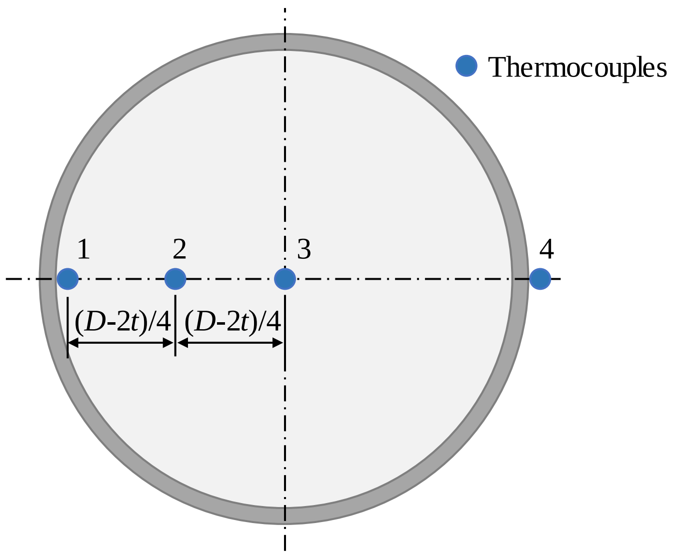


(a) Schematic diagram of the thermocouple positions.

(b) Photograph

**Fig. 2.** Arrangement of thermocouples.

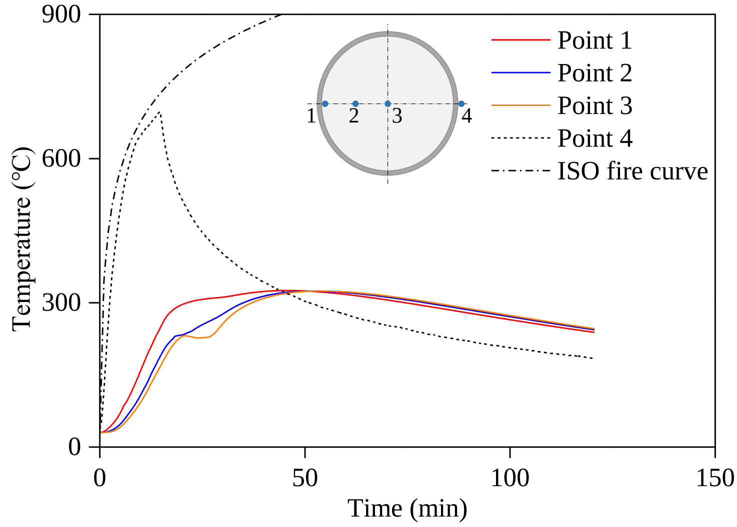


(a) D73-C90-T15

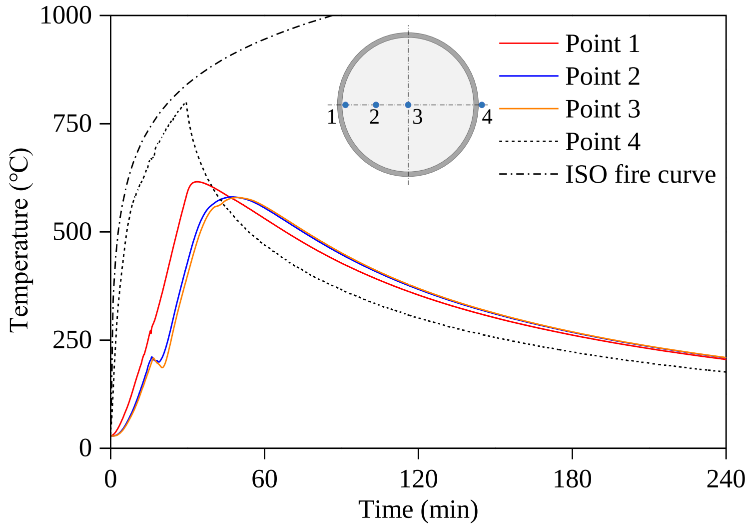


(b) D73-C90-T30

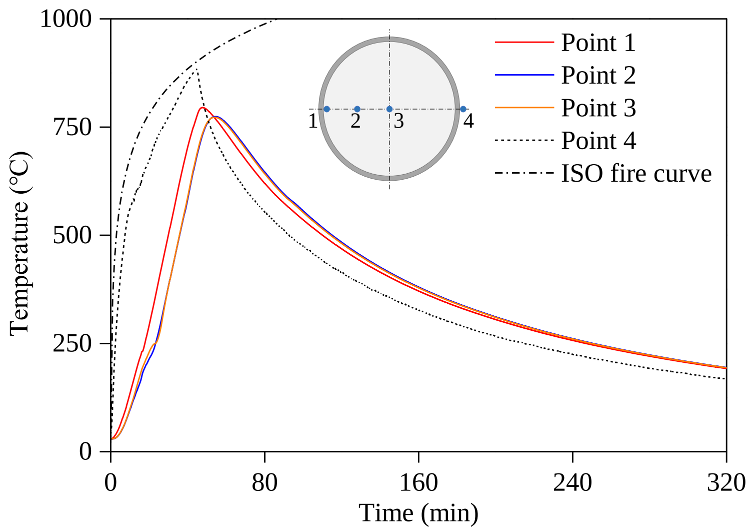


(c) D73-C90-T45

**Fig. 3.** Temperature–time curves for HCFSST stub column specimen series D73-C90.

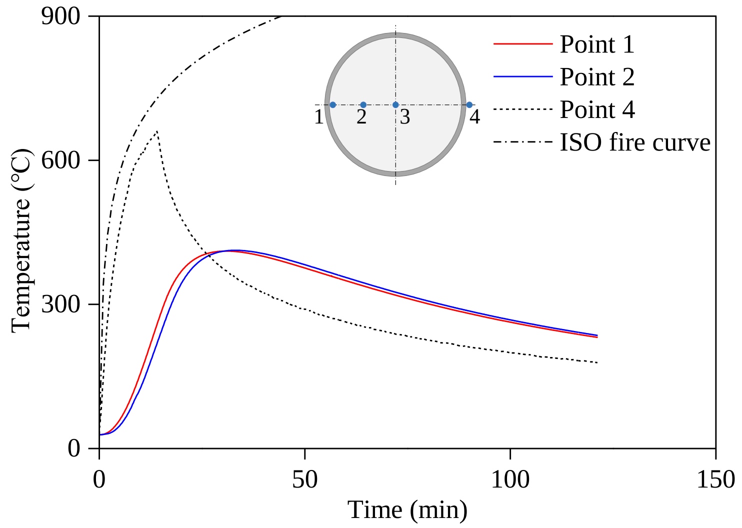


(a) D73-C140-T15

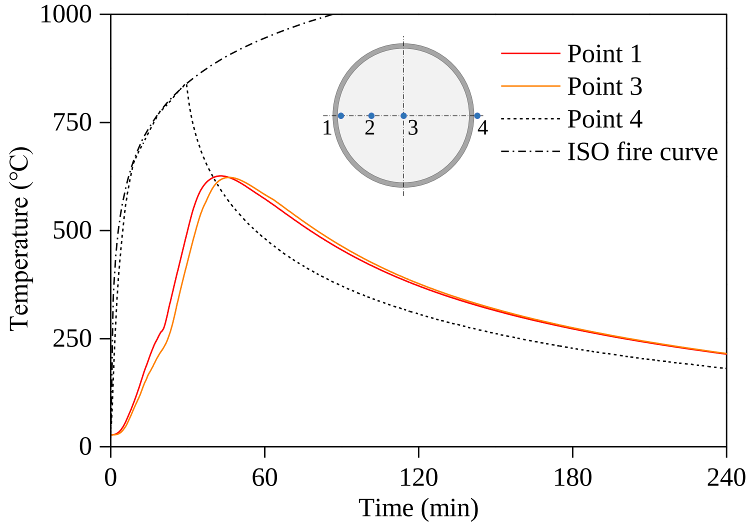


(b) D73-C140-T30

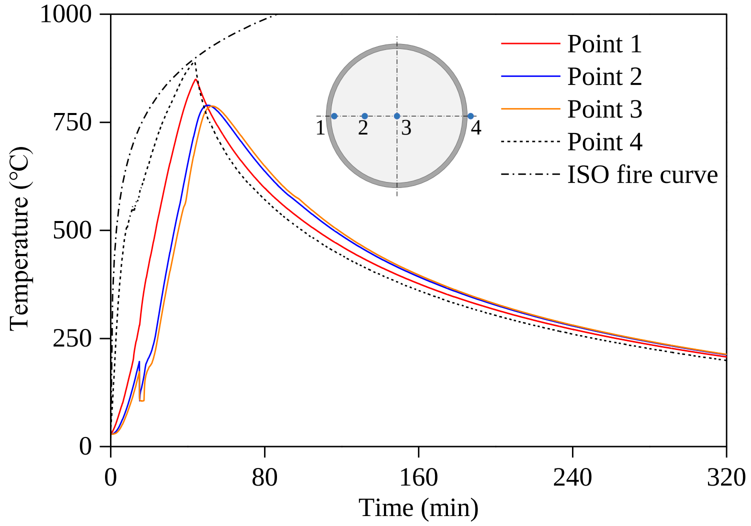


(c) D73-C140-T45

**Fig. 4.** Temperature–time curves for HCFSST stub column specimen series D73-C140.

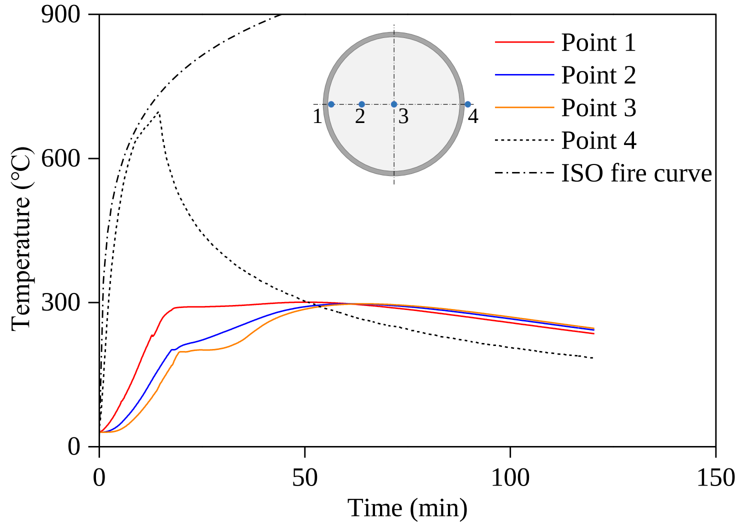


(a) D89-C90-T15

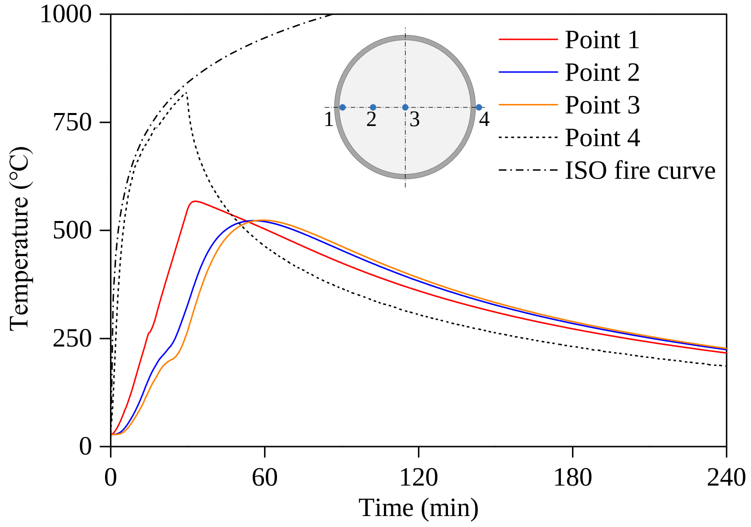


(b) D89-C90-T30

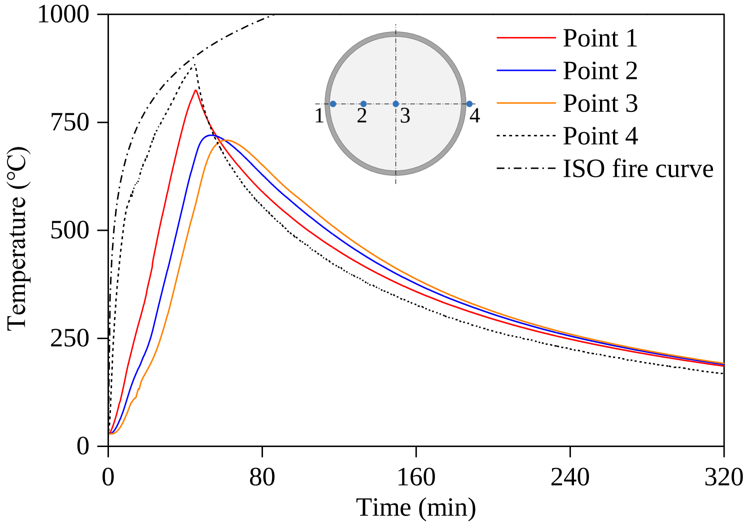


(c) D89-C90-T45

**Fig. 5.** Temperature–time curves for HCFSST stub column specimen series D89-C90.

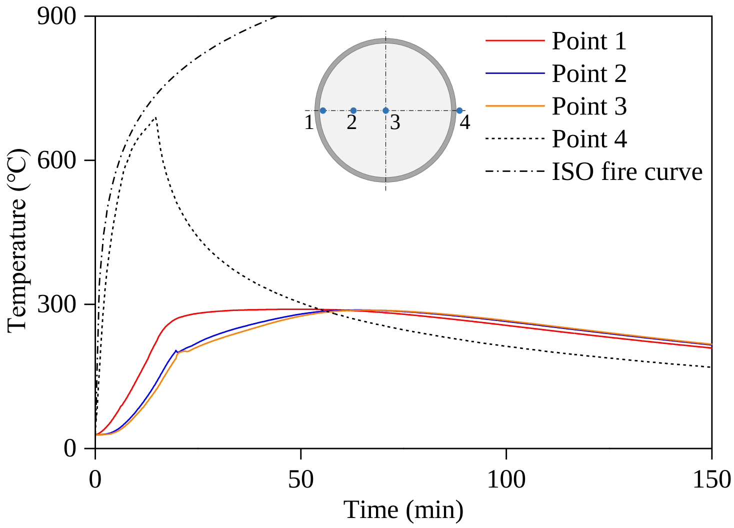


(a) D89-C140-T15

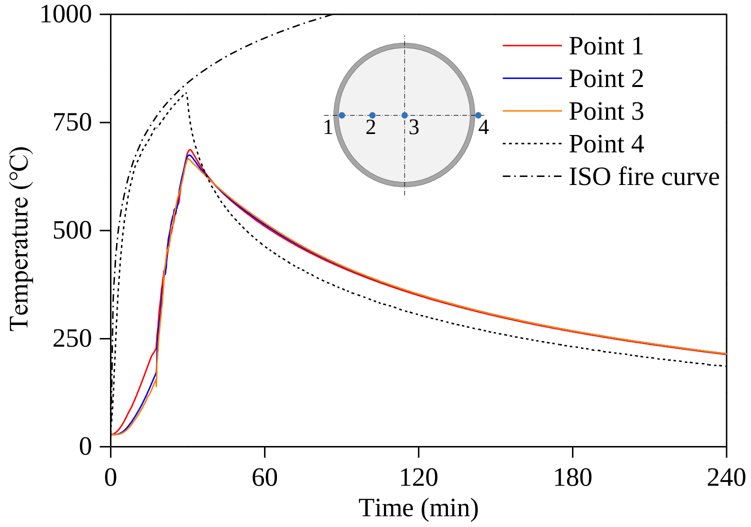


(b) D89-C140-T30

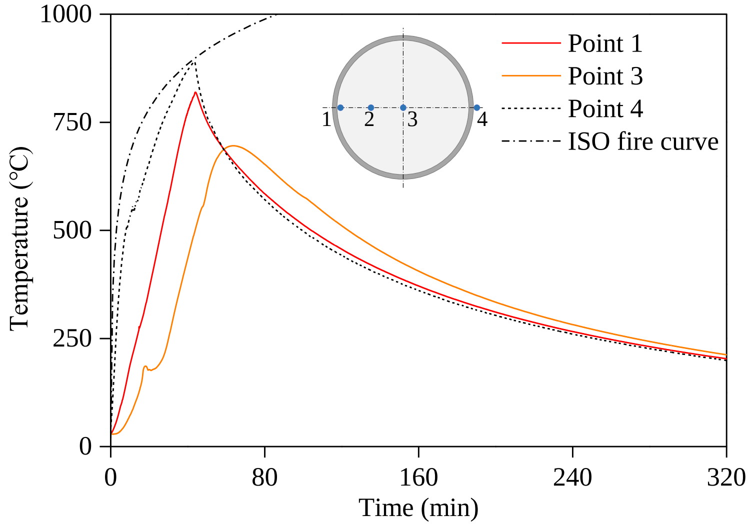


(c) D89-C140-T45

**Fig. 6.** Temperature–time curves for HCFSST stub column specimen series D89-C140.


**Fig. 7.** Colours of austenitic stainless steel tensile coupons after exposure to the ISO-834 standard fire for different levels of heating durations.

(a) D89-C140-T0 (b) D89-C140-T15 (c) D89-C140-T30 (d) D89-C140-T45

**Fig. 8.** Colours of concrete cores after exposure to the ISO-834 standard fire for different levels of heating durations.

**Fig. 9** Tensile coupon test rig

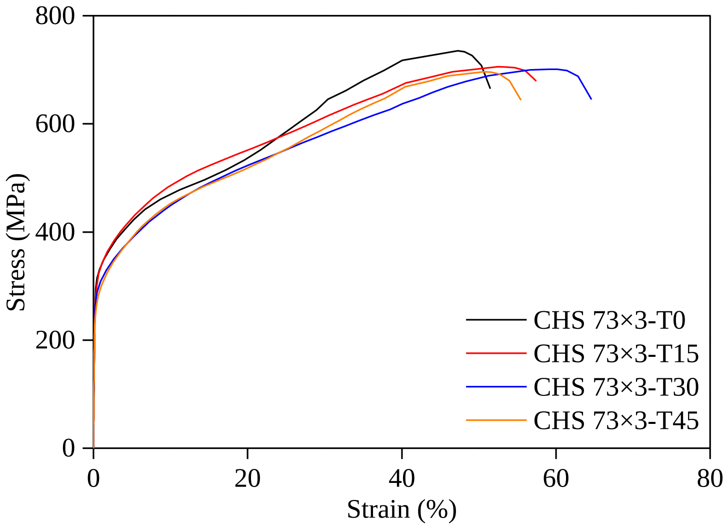


(a) CHS 73×3

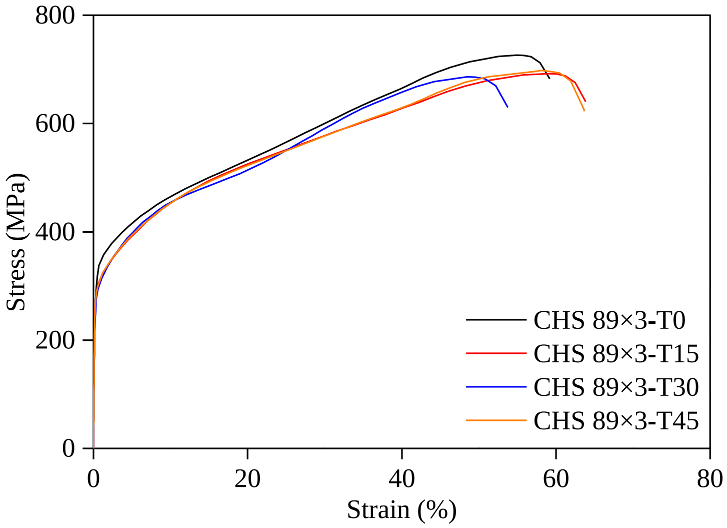


(b) CHS 89×3

**Fig. 10.** Stress–strain curves of austenitic stainless steel after exposure to the ISO-834 standard fire for different levels of heating durations.

**Fig. 11.** Stub column test setup.

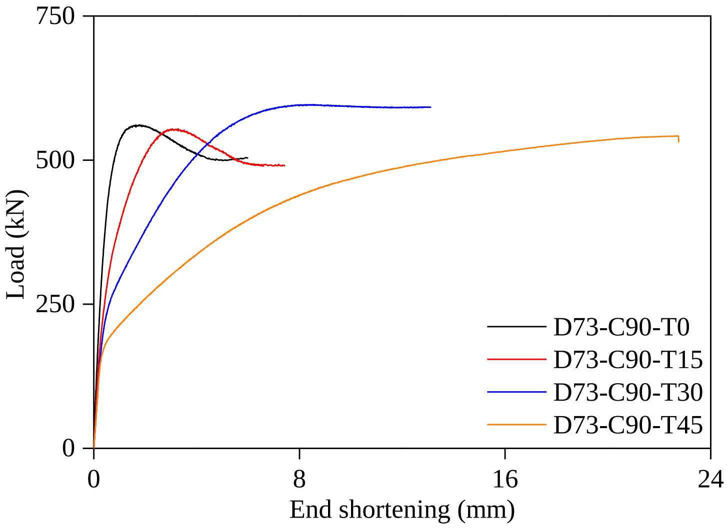


(a) Specimen series D73-C90

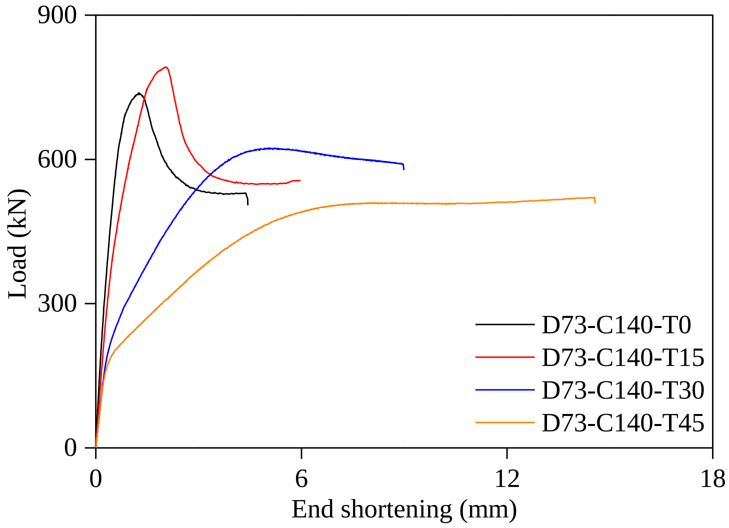


(b) Specimen series D73-C140

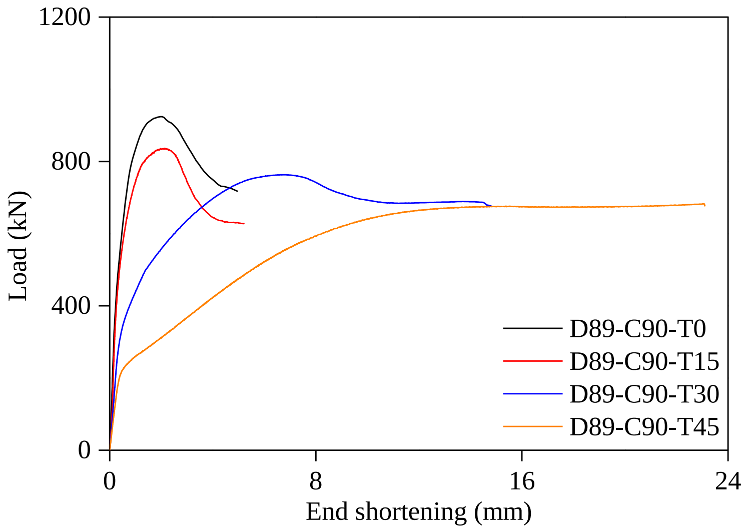


(c) Specimen series D89-C90

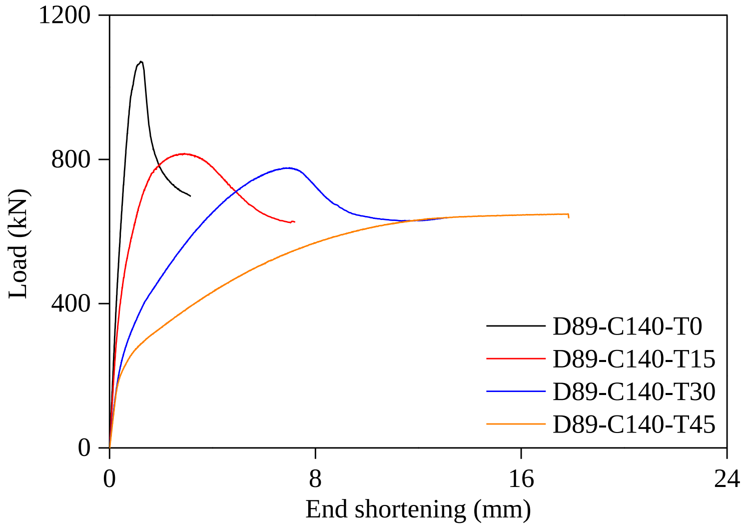


(d) Specimen series D89-C140

**Fig. 12.** Load–end shortening curves of HCFSST stub column specimens after exposure to the ISO-834 standard fire for different levels of heating durations.

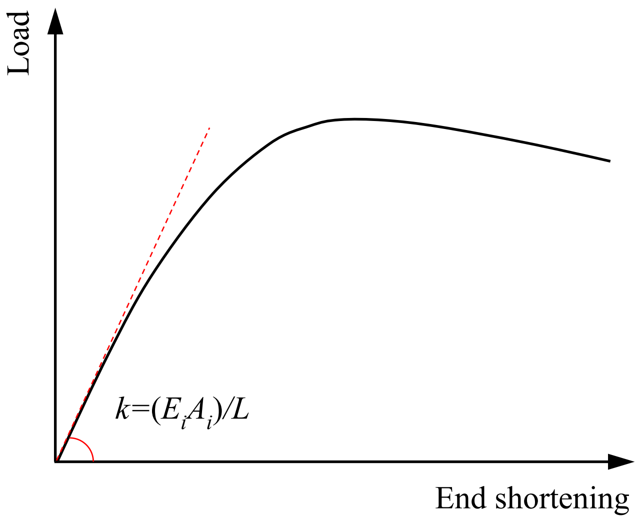


**Fig. 13.** Definition of initial compressive stiffness.

(a) Experimental failure modes.

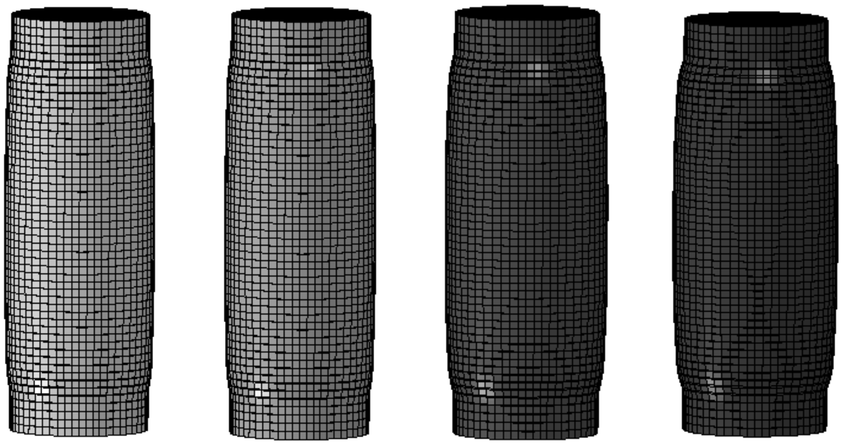

D89-C90-T0 D89-C90-T15 D89-C90-T30 D89-C90-T45

(b) Numerical failure modes.

**Fig. 14.** Experimental and numerical failure modes for specimen series D89-C90.

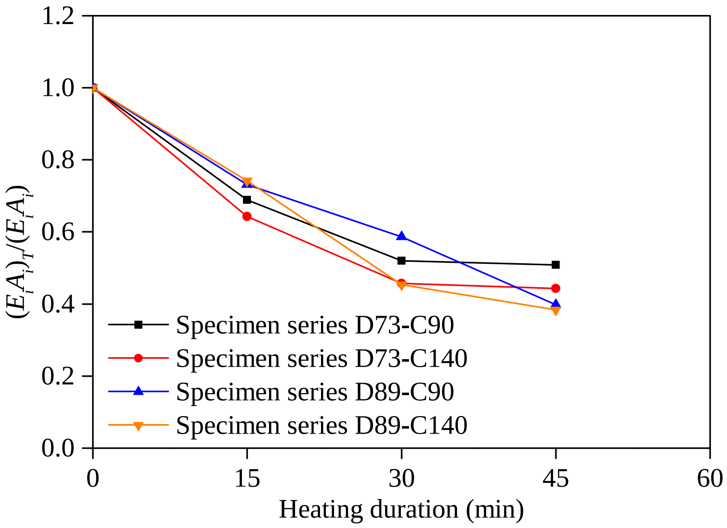


(a) $(E_iA_i)_T/(E_iA_i)$

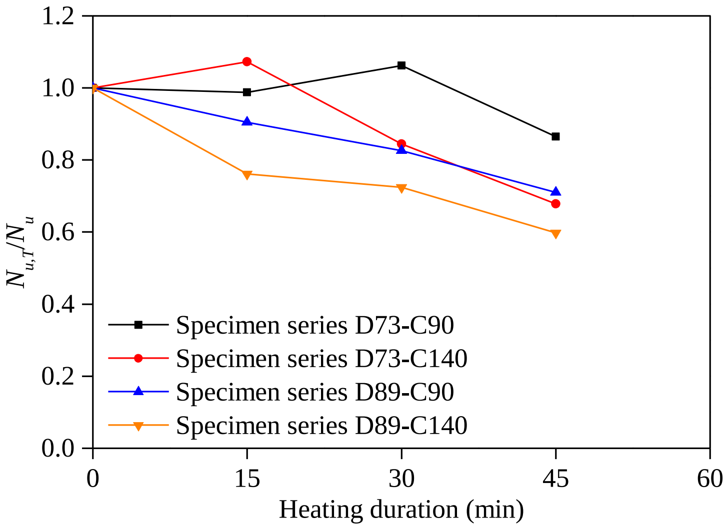


(b) $N_{u,T}/N_u$

**Fig. 15.** Reduction factors of initial compressive stiffness and ultimate compression resistance.

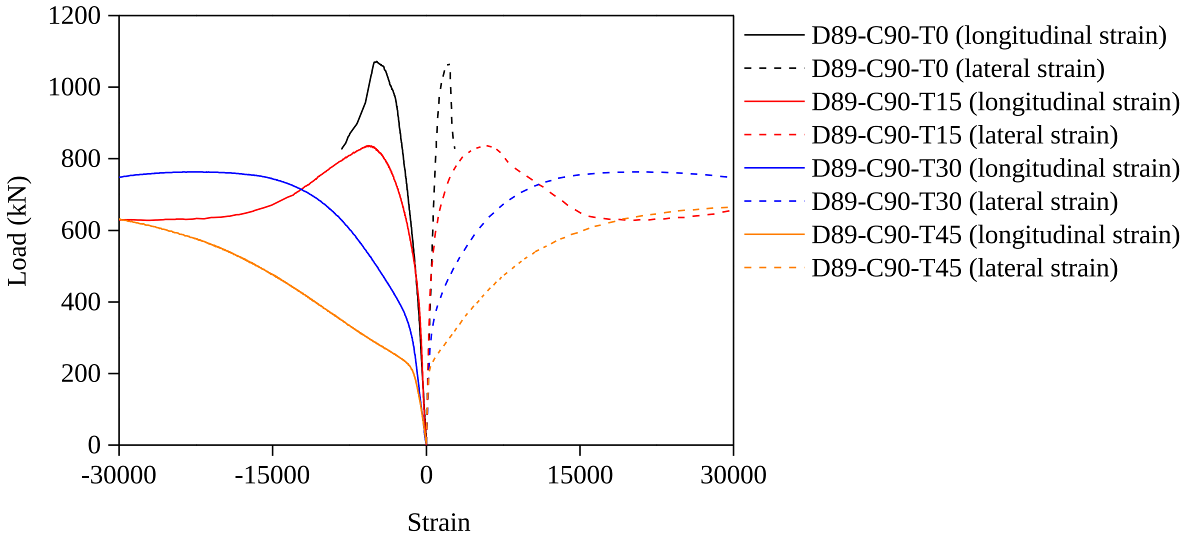


**Fig. 16.** Load–strain curves measured from specimen series D89-C90.

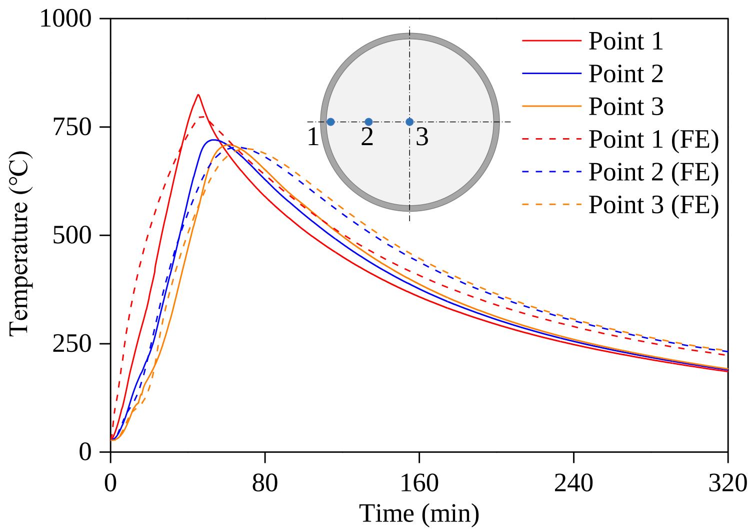


**Fig. 17.** Experimental and numerical temperature−time curves for specimen D89-C90-T45.

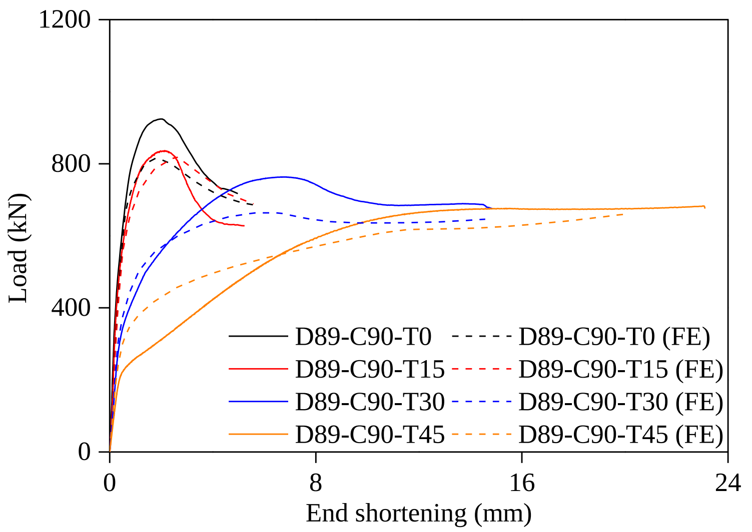


**Fig. 18.** Experimental and numerical load−end shortening curves for specimen series D89-C90.

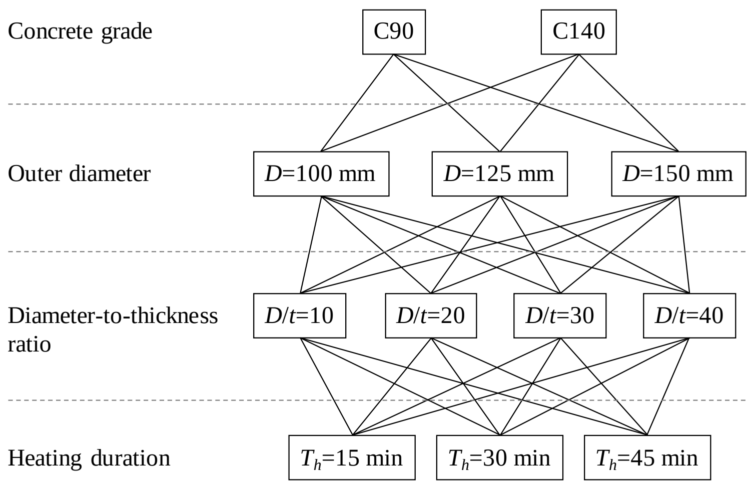


**Fig. 19.** Geometric dimensions, material properties and heating durations selected for parametric studies.

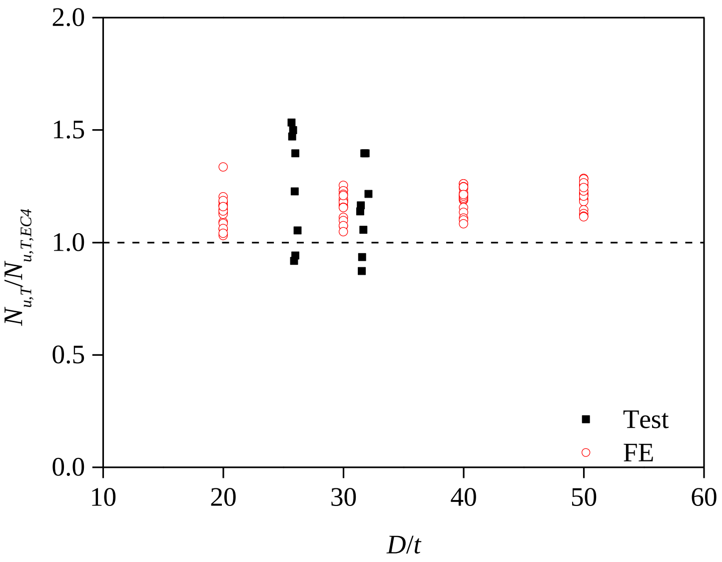


**Fig. 20.** Comparison of test and FE results with EC4 resistance predictions.

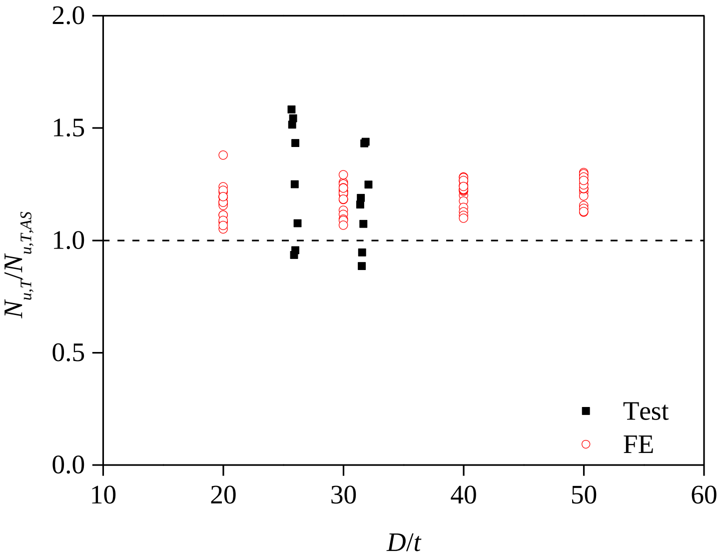


**Fig. 21.** Comparison of test and FE results with AS resistance predictions.

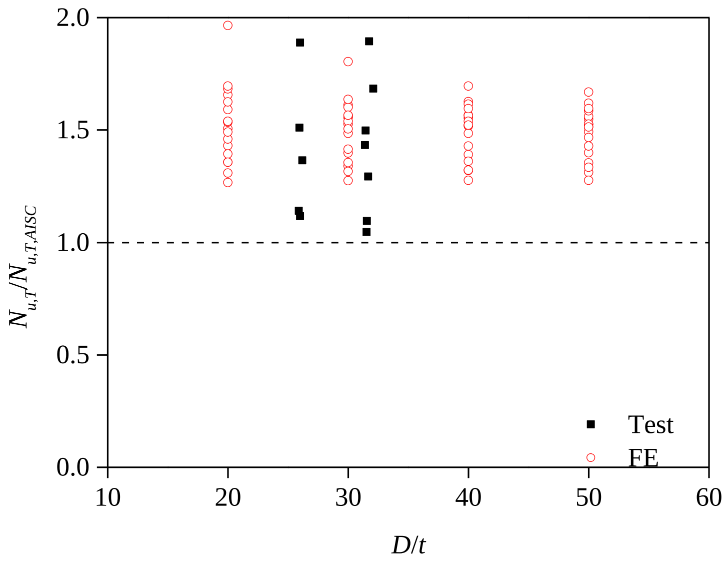


**Fig. 22.** Comparison of test and FE results with AISC resistance predictions.